Inorganic Chemistry

Article

pubs.acs.org/IC

Series of SHG Materials Based on Lanthanide Borate−Acetate Mixed Anion Compounds

Hui Yang,[†,‡] Chun-Li Hu,[†] Xiang Xu,[†] and Jiang-Gao Mao*[,†]

[†]State Key Laboratory of Structural Chemistry, Fujian Institute of Research on the Structure of Matter, Chinese Academy of Sciences, Fuzhou 350002, P. R. China

[‡]University of the Chinese Academy of Sciences, Beijing 100039, P. R. China

Supporting Information

ABSTRACT: The first examples of lanthanide borate−acetate mixed anion compounds, namely, $Ln_2(CH_3CO_2)_2[B_5O_9(OH)]\cdot H_2O$ (Ln = La **1**; Ce **2**; Pr **3**), were synthesized under hydrothermal conditions. These compounds are isostructural and crystallize in polar space group *Cc*. They display a unique three-dimensional (3D) framework built by a 3D network of lanthanide borate further decorated by acetate anions. The borate anion exhibits a 2D layer in the *ac* plane with large 9-member rings (MRs) which are filled by lanthanide(III) ions into a $\{Ln[B_5O_9(OH)]\}^-$ 2D layer. Adjacent $\{Ln[B_5O_9(OH)]\}^-$ layers are bridged by remaining lanthanide (III) ions to form a 3D network of lanthanide borate. It is noteworthy that $Ln_2(CH_3CO_2)_2[B_5O_9(OH)]\cdot H_2O$ (Ln = La **1**; Ce **2**; Pr **3**) can be changed into $Ln_2(CH_3CO_2)_2[B_5O_9(OH)]$ (Ln = La **4**; Ce **5**; Pr **6**) under heating at 500 K. Compounds **1**−**4** display moderate SHG signals of about 2.0, 1.0, 1.4, and 2.5 times that of KH_2PO_4, respectively, and they are phase matchable. Their SHG responses mainly arise from the synergistic polarization effects of both asymmetric borate clusters and π-conjugated CH_3COO^- anions.

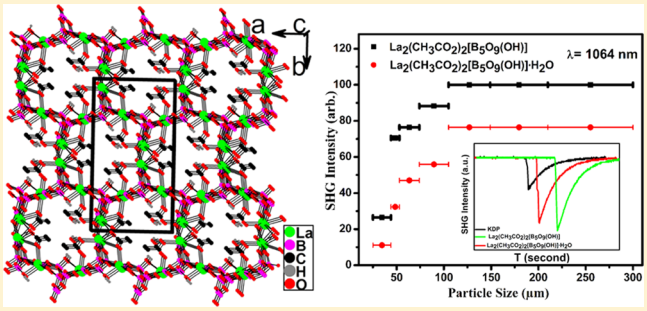

INTRODUCTION

Nonlinear optical (NLO) materials play a prominent role in photonic technologies.[1] The borates family is especially important in practical application as UV NLO crystals, due to their wide transmittance, high optical damage thresholds, and considerably large second-order NLO responses.[2,3] Over the last 30 years, intensive studies on metal borates have resulted in the discoveries of many NLO crystals including β-BaB_2O_4(BBO), LiB_3O_5(LBO), and $CsLiB_6O_{10}$(CLBO).[4] Recently, it has been demonstrated that new borate NLO compounds can be designed by introducing another π-conjugated planar triangular anionic unit such as NO_3^- and CO_3^{2-} anions which are isoelectronic with BO_3^{3-} anion into metal borates.[5] This has led to the discoveries of $Pb_2(BO_3)(NO_3)$[6a] and $Pb_7O(OH)_3(CO_3)_3(BO_3)$,[6b] which exhibit large SHG signals of 9.0 × and 4.5 × KDP (KH_2PO_4), respectively.

NLO materials based on coordination compounds have also been widely explored recently.[7−9] To target coordination compounds with noncentrosymmetric (NCS) structures, which is a prerequisite for second-order NLO materials, researchers have systematically developed numerous synthetic methods such as molecular self-assembling, taking advantage of metal−ligand coordination bonds, and incorporating chiral organic building ligands, etc.[10] A large number of SHG-active coordination compounds have been isolated including $C_6H_{15}N_4O_6Re$,[11] $[NH_4][Cd(HCOO)_3]$,[12] Cd(Imazethapyr)$_2$],[13] and $Eu_2L\cdot 2DMF$.[9] For the SHG-active materials reported, the large SHG signals mostly arise from the π-conjugated effect of organic ligands which could lead to large second-order NLO susceptibility.[14] However, for metal complexes with achiral ligands, it is still a great challenge to achieve NCS structures. Our hypothesis is that if we can introduce rigid asymmetric borate clusters into those coordination compounds to get inorganic−organic hybrid materials, we can not only greatly increase the probability to obtain NCS materials but also enhance their thermal stabilities and SHG responses because of the synergistic effect of the two types of SHG-active groups.[15] In this regard, so far a few NCS metal borate-carboxylates have been reported, for example, $ASr[C_4H_2O_6B(OH)_2]\cdot 64H_2O$ (A = K^+, Rb^+)[16] with SHG responses of 1.5 and 1.7 × KDP, respectively, and RbB(DL-$C_4H_4O_5$) displaying a SHG response of about 2.0 × KDP.[17] However, in both compounds, the borate group and carboxylate ligand are condensed into a new type of organic ligand containing a BO_4 group. To the best of our knowledge, no borate−acetate mixed anion compounds have yet been reported. Lanthanide complexes and lanthanide borates have also been widely studied due to their unique optical properties.[18−21] Our explorations of NCS hybrid materials in the Ln_2O_3−B_2O_3−CH_3COOH system led to the isolation of the first examples of polar borate−acetate mixed anion

Received: May 19, 2015
Published: July 21, 2015

DOI: 10.1021/acs.inorgchem.5b01126
Inorg. Chem. 2015, 54, 7516−7523

Table 1. Crystal Data and Structure Refinements for Six Compounds

	compound 1	compound 2	compound 3	compound 4	compound 5	compound 6
temperature	298 K	298 K	298 K	500 K	500 K	500 K
fw	628.98	631.40	632.98	610.97	613.39	614.97
space group	*Cc*	*Cc*	*Cc*	*Cc*	*Cc*	*Cc*
a (Å)	10.7704	10.7454	10.6898	10.9596	10.9510	10.9265
b (Å)	20.1471	20.0674	19.9883	20.2634	20.2411	20.2045
c (Å)	6.4727	6.4580	6.4273	6.4760	6.4535	6.4365
α (deg)	90	90	90	90	90	90
β (deg)	90.582	90.527	90.545	90.540	90.494	90.528
γ (deg)	90	90	90	90	90	90
V (Å^3)	1404.45	1392.49	1373.25	1438.12	1430.43	1420.89
Z	4	4	4	4	4	4
D_{calcd} (g·cm^{-3})	2.975	3.012	3.062	2.822	2.848	2.875
μ (mm^{-1})	6.087	6.541	7.099	5.935	49.284	52.707
F(000)	1168	1176	1184	1128	1136	1144
GOF on F^2	1.082	1.083	1.059	1.023	1.075	1.029
R_1, wR_2 ($I > 2y(I)$)[a]	0.0622, 0.1560	0.0573, 0.1418	0.0685, 01620	0.0400, 0.0767	0.0522, 0.1303	0.0436, 0.1050
R_1, wR_2 (all data)	0.0652, 0.1615	0.0603, 0.1449	0.0748, 0.1697	0.0455, 0.0813	0.0542, 0.1336	0.0482, 0.1096

[a] $R_1 = \sum||Fo| - |Fc||/\sum|Fo|$, $wR_2 = \{\sum w[(Fo)^2 - (Fc)^2]^2/\sum w[(Fo)^2]^2\}^{1/2}$.

compounds, namely, $Ln_2(CH_3CO_2)_2[B_5O_9(OH)]\cdot H_2O$ (Ln = La **1**; Ce **2**; Pr **3**). Upon dehydration, $Ln_2(CH_3CO_2)_2[B_5O_9(OH)]\cdot H_2O$ (Ln = La **1**; Ce **2**; Pr **3**) can be changed into $Ln_2(CH_3CO_2)_2[B_5O_9(OH)]$ (Ln = La **4**; Ce **5**; Pr **6**). Compounds **1**−**4** exhibit moderate SHG responses. Herein, we study their hydrothermal syntheses, single crystal structures, SHG and ferroelectric properties.

EXPERIMENTAL SECTION

Reagents and Physical Measurements. $(NH_4)_2B_{10}O_{16}\cdot 8H_2O$ (Aladdin, 99.9%), Ln $(CH_3CO_2)_3\cdot nH_2O$ (Ln = La, Ce; Aladdin, 99.9%), acetic acid (Sinopharm, 99.5%), H_3BO_3 (Shanghai Reagent Factory, 99.9%), and Pr_2O_3 (Alfa Aesar, 99.99 +%) were employed as received. Powder XRD analyses were recorded on a XPERT−MPD θ−2θ diffractometer equipped with Cu Kα radiation in the angular range from 5 to 55° (2θ) with a step width of 0.02° for 30 min at room temperature. IR spectra were performed from 4000 to 400 cm^{-1} on a Magna 750 FT−IR spectrometer using KBr pellets at room temperature. The inductively coupled plasma (ICP) elemental analyses on Ln and B for lanthanide and boron elements were measured using an Ultima 2 simultaneous inductively coupled plasma optical emission spectrometer. Elemental analyses on C and H were taken on a German Elementary Vario EL III instrument. Optical diffuse−reflectance spectra were recorded with the aid of a PE Lambda 900 UV−visible spectrophotometer at room temperature. Thermogravimetric analyses (TGA) and differential scanning calorimetry (DSC) analyses were performed on a NETZSCH 449C thermal analyzer instrument at a heating rate of 10 °C/min under N_2 atmosphere in the temperature range of 30−1000 °C. Measurements of the powder frequency−doubling effect were carried out by the modified method of Kurtz and Perry.[22] Measurements were carried out at 1064 and 532 nm laser radiation for visible and ultraviolet SHG, respectively. Sieved KDP and BBO samples (150−210 μm) were taken as references for assuming SHG signals. The samples were ground and sieved into several distinct particle size ranges (25−45, 45−53, 53−75, 75−105, 105−150, 150−210, and 210−300 μm) to check whether they were phase-matching or not. The ferroelectric properties for compounds **1**−**4** were carried out on an aixACCT TF Analyzer 2000E ferroelectric tester at 298 K. The powder samples were pressed into pellets under 20 MPa pressure and the pellets were further treated by cool isostatic pressing to make them denser. The conducting Ag glue was applied on the both sides of the pellet surfaces for electrodes without further treatments. The theoretical densities for four pellets are given according to single-crystal X-ray studies, while the actual densities are obtained based on $\rho = m/V$. The actual, theoretical, and relative densities of four pellets are listed in Supporting Information (SI) Table S1.

Preparation of $Ln_2(CH_3CO_2)_2[B_5O_9(OH)]\cdot H_2O$ (Ln = La 1; Ce 2; Pr 3) and $Ln_2(CH_3CO_2)_2[B_5O_9(OH)]$ (Ln = La 4; Ce 5; Pr 6). Single crystals of compounds **1**−**3** were obtained through hydrothermal reactions. The loaded reactive mixtures were $La(CH_3CO_2)_3\cdot nH_2O$ (0.3688 g, 1.2 mmol), $(NH_4)_2B_{10}O_{16}\cdot 8H_2O$ (0.4723 g, 0.86 mmol), and H_2O (5 mL) for compound **1**; $Ce(CH_3CO_2)_3\cdot nH_2O$ (0.2771g, 0.87 mmol), $(NH_4)_2B_{10}O_{16}\cdot 8H_2O$ (0.2821g, 0.52 mmol), and H_2O (2 mL) for compound **2**; Pr_2O_3 (0.3688 g, 1.12 mmol), $(NH_4)_2B_{10}O_{16}\cdot 8H_2O$ (0.4723 g, 0.86 mmol), CH_3COOH (2 mL), and H_2O (2 mL) for compound **3**. The resulting mixtures were introduced into a Teflon-lined stainless steel autoclave (23 mL) and heated at 220 °C for 4 days for compounds **1** and **3**, or 210 °C for 3 days for compound **2**. After cooling to 25 °C, rod crystals were obtained by washing the product with deionized water. The yields of compounds **1**−**3** were 80%, 50%, and 75% based on La, Ce, and Pr, respectively. Crystals of compounds **4**−**6** were obtained by heating their corresponding hydrated species at 300 °C for 10 h. Anal. Calcd for $La_2(CH_3CO_2)_2[B_5O_9(OH)]\cdot H_2O$ (Mr = 628.98): La, 44.16; B, 8.59; C, 7.64; H, 1.43. Found: La, 44.58; B, 9.00; C, 7.46; H, 1.43%. Anal. Calcd for $Ce_2(CH_3CO_2)_2[B_5O_9(OH)]\cdot H_2O$ (Mr = 631.40): Ce, 44.38; B, 8.56; C, 7.58; H, 1.43. Found: Ce, 44.00; B, 8.93; C, 7.40; H, 1.43%. Anal. Calcd for $Pr_2(CH_3CO_2)_2[B_5O_9(OH)]\cdot H_2O$ (Mr = 632.98): Ce, 44.38; B, 8.56; C, 7.58; H, 1.43. Found: Pr, 44.88; B, 9.32; C, 7.54; H, 1.42%. Anal. Calcd for $La_2(CH_3CO_2)_2[B_5O_9(OH)]$ (Mr = 610.97): La, 45.47; B, 8.84; C, 7.86; H, 1.15. Found: La, 45.05; B, 8.90; C, 7.80; H, 1.20%. Their purities were confirmed by PXRD studies (SI Figure S1). IR data (KBr cm^{-1}): 3414 (m), 1671 (w), 1563 (s), 1417 (s), 1335 (s), 1063 (s), 941 (m), 738 (s), 605 (m) for compound **1**; 3433 (s), 1672 (m), 1575 (s), 1414 (s), 1325 (s), 1255 (s), 943 (w), 721 (w), 658 (w) for compound **2**; 3424 (s), 1681 (m), 1584 (s), 1423 (s), 1255 (s), 1077 (s), 952 (w), 739 (w), 614 (w) for compound **3**; 3421 (s), 1557 (s), 1416 (s), 1331 (s), 1248 (s), 1043 (s), 945 (w), 738 (w), 606 (w) for compound **4**. Because not enough samples were available, characterizations of compounds **5** and **6** were limited to single crystal XRD studies.

Crystal Structure Determination. Data for **1**−**3** were collected using SuperNova X-ray Source, Mo Kα/ Cu radiation at room temperature. Data collection of three compounds at 298 and 500 K revealed that there is single-crystal-to-single-crystal (SCSC) dehydration procedure and $Ln_2(CH_3CO_2)_2[B_5O_9(OH)]\cdot H_2O$ (Ln = La **1**; Ce **2**; Pr **3**) can be changed into $Ln_2(CH_3CO_2)_2[B_5O_9(OH)]$ (Ln = La **4**; Ce **5**; Pr **6**). All data sets were corrected for Lorentz and polarization factors, as well as for absorption by the multiscan

DOI: 10.1021/acs.inorgchem.5b01126
Inorg. Chem. 2015, 54, 7516−7523

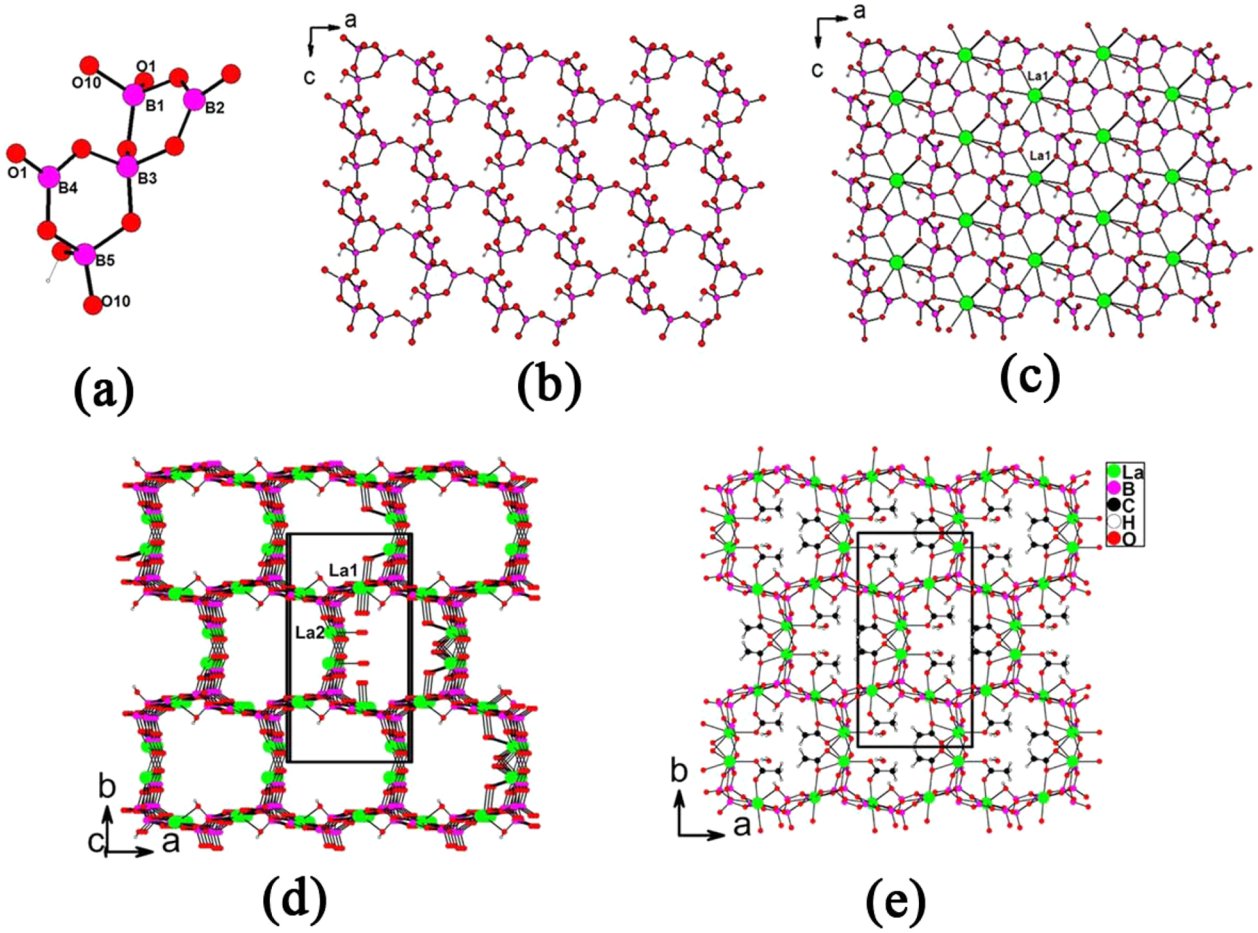

Figure 1. $[B_5O_{11}(OH)]^{8-}$ cluster unit (a), a 2D $[B_5O_9(OH)]^{4-}$ borate layer (b), a 2D La(1)$[B_5O_9(OH)]^{-}$ layer (c), view of the 3D network of lanthanum borate down the *c*-aixs (d), and view of the structure of $La_2(CH_3CO_2)_2[B_5O_9(OH)]\cdot H_2O$ down the *c*-axis (e). The B, C, La, and O atoms are drawn as purple, black, green, and red circles, respectively.

method.[23a] Six structures were solved by direct methods and refined by a full−matrix least−squares fitting on F^2 by SHELX−97.[23b] All hydrogen atoms are located at geometrically calculated positions and refined with isotropic thermal parameters. The refined Flack factors are −0.02(5), −0.02(5), −0.06(5), −0.07(3), −0.033(13), and −0.019(10) for compounds **1**−**6**, respectively, which are all close to zero, confirming the correctness of their absolute structures. By the program PLATON, all six structures were also checked for possible missing symmetry and none were found.[23c] Crystal data, the information on structural refinement of all compounds, are reported in Table 1. More information on the crystal studies are provided in the Supporting Information.

Computational Method. The electronic and SHG properties of compound **4** were calculated using DFT method within CASTEP.[24] In our calculations, the GGA-PBE was chosen as the exchange-correlation function.[25] Norm-conserving pseudopotential was used to treat the electron−core interactions.[26] The outmost electrons of B, C, O, and H, as well as La-$5d^16s^2$ were considered as valence electrons. A 2 × 1 × 4 *k*-point sampling and a 750-eV cutoff energy were adopted to determine the numerical integration and plane wave numbers, respectively. Two hundred seventy-two empty bands were contained in the optical property calculations to make the real SHG coefficients effectively converge.

For the calculation of second-order NLO susceptibilities, we adopted the static formula put forward by Lin,[27] which has been proven to be more accurate by numerous previous reports for treating the borates.

RESULTS AND DISCUSSION

Hydro-thermal reactions of lanthanide acetates with $(NH_4)_2B_{10}O_{16}\cdot 8H_2O$ at 220 or 210 °C resulted in the preparation of a series of lanthanide(III) borate−acetate hybrid materials, namely, $Ln_2(CH_3CO_2)_2[B_5O_9(OH)]\cdot H_2O$ (Ln = La **1**; Ce **2**; Pr **3**). It is interesting to note that compounds **1**−**3** were changed into compounds $Ln_2(CH_3CO_2)_2[B_5O_9(OH)]$ (Ln = La **4**; Ce **5**; Pr **6**) after heating at 300 °C for 10 h. These compounds represent the first lanthanide acetates containing borate cluster anions. They display novel frameworks and intriguing optical properties, especially second harmonic generations.

Structural Description. $Ln_2(CH_3CO_2)_2[B_5O_9(OH)]\cdot H_2O$ (Ln = La **1**; Ce **2**; Pr **3**) and $Ln_2(CH_3CO_2)_2[B_5O_9(OH)]$ (Ln = La **4**; Ce **5**; Pr **6**) crystallize in the polar monoclinic space group *Cc*. Because all six compounds display similar 3D network structures, the structure of compound **1** is described in detail as a representative. The asymmetric unit of $La_2(CH_3CO_2)_2[B_5O_9(OH)]\cdot H_2O$ contains two La^{3+} ions, one $[B_5O_9(OH)]^{4-}$ cluster, two CH_3COO^- ions, and one lattice water molecule. The fundamental building block (FBB) of the polyborate anion is $[B_5O_{11}(OH)]^{8-}$, composed of one B_3O_8 and one $B_3O_7(OH)$ group sharing a common BO_4 group. Similar such borate clusters have been reported in other metal borates (Figure 1a).[28] Each $[B_5O_{11}(OH)]^{8-}$ cluster is bonded with four neighboring ones through corner-sharing (O(1) and

DOI: 10.1021/acs.inorgchem.5b01126
Inorg. Chem. 2015, 54, 7516−7523

O(10) atoms) into a 2D layer in the *ac* plane which displays 9-member rings (MRs) (Figure 1b). The BO_3 groups have B−O distances in the range from 1.315(16) to 1.405(17) Å and O−B−O angles locating between 116.5(10) and 124.3(11) °. For the BO_4 tetrahedra, B−O distances and O−B−O angles are in the range 1.425(14)−1.534(17) Å and 103.3(9)−116.3(10) °, respectively. All of these values are consistent with those acquired from other borates.[4−6] Among the two unique lanthanum atoms, La(1) resides in the 9-member rings of the borate layer and it is nine-coordinated by seven borate oxygen atoms and two unidentate acetate anions, whereas La(2) is nine-coordinated by five borate oxygens and three acetate anions (two in unidentate chelating fashion and one in bidentate fashion) (SI Figure S2). The La−O bond lengths range from 2.377(9) to 2.788(9) Å corresponding to those observed in other lanthanum borates.[17−20] The bond valence sum (BVS) calculations for La(1), La(2), and B(1)−B(5) atoms gave value of 3.24, 2.96, 3.04, 3.05, 3.06, 3.10, and 3.07, respectively, resulting in oxidation states of +3 for La and B atoms.[28]

The interconnection of La(1) and borate clusters led to a 2D $\{Ln[B_5O_9(OH)]\}^-$ layer (Figure 1c). Adjacent $\{Ln[B_5O_9(OH)]\}^-$ layers were bridged by La(2) atoms into a 3D $\{Ln_2[B_5O_9(OH)]\}^{2+}$ network with 1D tunnels of large La_4B_{12} 16-MRs along the *c* axis (Figure 1d). The acetate anions are grafted on the walls of 1D tunnels of the above La_4B_{12} 16-MRs whereas the lattice waters are resided in the 1D tunnels (Figure 1e). The acetate anion containing C(1), C(2), O(11) and O(12) is tetradentate and it forms a bidentate chelation with a La(2) atom and also bridges with two other La atoms. The other acetate anion adopts a bidentate bridging coordination mode (SI Figure S3a). The interconnection of lanthanum(III) ions by acetate anions leads to a 3D network with large 1D tunnels along the *c* axis (SI Figure S3b).

The lattice water forms several hydrogen bonds with borate oxygen atoms (O(9)−H(9A)···O(1W) 2.789 Å; O(1W)−H(1WA)···O(13) 2.796 Å; O(1W)−H(1WB)···O(13) 3.023 Å) providing additional stability in this structure.

Comparison of the structure of $La_2(CH_3CO_2)_2[B_5O_9(OH)]\cdot H_2O$ with that of $Ca_2[B_5O_9](OH)\cdot H_2O$,[29] which also crystallizes in monoclinic space group *Cc*, revealed significant differences. Though both of the borate anions are based on B_5O_{12} unit, the $[B_5O_9(OH)]^{4-}$ in $La_2(CH_3CO_2)_2[B_5O_9(OH)]\cdot H_2O$ features a layered structure whereas the $[B_5O_9]^{3-}$ in $Ca_2[B_5O_9](OH)\cdot H_2O$ is 3D *pcu* net with nine-member ring (9-MR) channels along the *b*-axis, where the Ca^{2+} cations, OH^- anions, and H_2O molecules are resided. Each B_5O_{12} unit connects with four neighbors in $La_2(CH_3CO_2)_2[B_5O_9(OH)]\cdot H_2O$, whereas each B_5O_{12} unit connects with six neighbors in $Ca_2[B_5O_9](OH)\cdot H_2O$. The reduction of dimensionality for the $[B_5O_9(OH)]^{4-}$ anion is due to the protonation of one oxygen, hence fewer intercluster B−O−B bridges are available.

Because of the decreasing of lanthanide ionic radii, the cell volumes and the three axial lengths decrease from compound **1** to compound **3** (Table 1). Data collection of compounds **1**−**3** at 500 K revealed that they are dehydrated and are changed to compounds **4**−**6**. The cell parameters (axial lengths and cell volume) of compounds **4**−**6** increase slightly compared with their parent compounds (Table 1), probably due to the thermal expansion.

TGA and DSC Studies. Thermogravimetric analyses (TGA) experiments under N_2 atmosphere reveal that compounds **1**−**3** are stable below 120, 114, and 130 °C, respectively (SI Figure S4). Then, they display weight losses in two steps. The weak weight losses occur from 120 to 200 °C for compound **1**, 140−290 °C for compound **2**, and 140−300 °C for compound **3**, corresponding to the loss of 1.0 H_2O per formula unit. The observed weight losses (2.96%, 2.50%, 2.41% for compounds **1**, **2**, and **3**, respectively) match well with the calculated ones (about 2.85%). The second step in the temperature range of 490−760, 500−750, 460−760 °C for compounds **1**, **2**, **3**, respectively, can be attributed to the decomposing of CH_3COO^- and borate units, and endothermic peaks around 740 °C in the DSC diagrams are observed. The weight losses are 16.05%, 16.39%, 17.46% for compounds **1**, **2**, **3**, respectively, which match well with the calculated ones (about 17.00% for all compounds) (SI Figure S4). The measured XRD powder patterns for the residuals of compound **1** upon calcination at 900 °C for 10 h reveal that they are mainly $LaBO_3$ (SI Figure S1a). TGA experiment indicates that $La_2(CH_3CO_2)_2[B_5O_9(OH)]$ (**4**) can be stable up to 500 °C (SI Figure S4d). There is one step of weight loss in the temperature range 500−750 °C attributed to the decomposition of CH_3COO^- anions and borate units. The total weight loss of 18.04% is close to the calculated value of 18.13%.

Single-crystal X-ray studies and TGA analyses of the crystals of $La_2(CH_3CO_2)_2[B_5O_9(OH)]$ exposed to water at room temperature for 2 days confirmed that it recovered to its original hydration state (SI Figure S4e). Therefore, compound **1** can be dehydrated and rehydrated reversibly.

Optical Properties. The UV absorption spectra illustrate that $Ln_2(CH_3CO_2)_2[B_5O_9(OH)]\cdot H_2O$ (Ln = La **1**; Ce **2**), and $La_2(CH_3CO_2)_2[B_5O_9(OH)]$ (**4**) have little absorption peaks from 300 to 2000 nm whereas $Pr_2(CH_3CO_2)_2[B_5O_9(OH)]\cdot H_2O$ (**3**) shows characteristic strong absorption bands around 436 nm of the Pr^{3+} ions which can be attributed to the f−f or f−d transition of Pr^{3+} ions.[30]

Optical diffuse reflectance spectrum measurements indicate that compounds **1**−**4** are wide band gap semiconductors displaying optical band gaps of 5.38, 4.02, 5.36, and 5.14 eV, respectively (SI Figure S5), which correspond to the UV cutoff edges at 230, 308, 231, and 240 nm, respectively. Different electronic configurations of the Ln^{3+} ions are responsible for the different band gaps of these isostructural materials.

Owing to the existence of H_2O molecules and/or OH^- groups, all compounds display broad absorption peaks centering at 3560 and 3430 cm^{-1}. The IR absorption peaks around 1675 cm^{-1} for compounds **1**−**3** are due to H−O−H bending mode, whereas there is no corresponding peak observed for compound **4** (SI Figure S6). Absorption bands ranging from 1557 to 1584 cm^{-1} could be associated with the asymmetric stretching of COO^-, and IR absorption peaks at around 1415 cm^{-1} could not be assigned undoubtedly for some overlaps of asymmetrical stretching of the BO_3 groups and the symmetric stretching of COO^- for all compounds. The peaks around 1250 cm^{-1} are also asymmetrical stretching of the BO_3 groups and the peaks of deformation vibrations of CH_3^- groups are at 1325−1343 cm^{-1}. The vibration absorption peaks around 1070 and 945 cm^{-1} can attribute to asymmetric stretching of BO_4 units. It is difficult to assign the absorption bands below 700 cm^{-1} because of the overlap of deformation vibration of COO^- and the bending modes of BO_4 groups in the low frequency vibrations for all compounds (SI Figure S6). These assignments are in accordance with other compounds reported previously.[4−6]

DOI: 10.1021/acs.inorgchem.5b01126
Inorg. Chem. 2015, 54, 7516−7523

SHG Measurements. The polar structures of $Ln_2(CH_3CO_2)_2[B_5O_9(OH)]\cdot H_2O$ (Ln = La, Ce, Pr) and $La_2(CH_3CO_2)_2[B_5O_9(OH)]$ prompt us to measure their SHG properties. SHG measurements under 1064 nm laser radiation in sieved particle size range 150−210 μm indicated that compounds **1**−**4** exhibit moderate SHG responses of 2.0, 1.0, 1.4, 2.5 × KDP, respectively. And they display SHG signals of about 0.33, 0.18, 0.23, 0.62 times of BBO, respectively, under laser radiation at 532 nm (Figure 2). For compounds **1** and **4**,

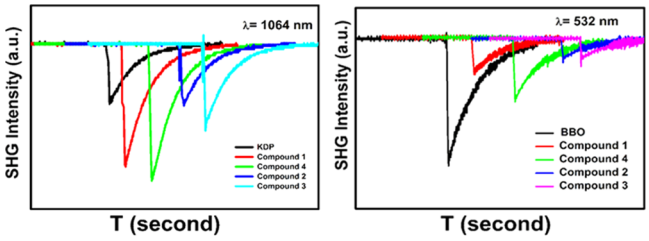

Figure 2. (a) Oscilloscope traces of the SHG signals for the powders of compounds **1**−**4** (149−210 μm) under a 1064 nm (a) and 532 nm (b) laser radiation. KDP and BBO were used as references for the SHG measurements at 1064 and 532 nm, respectively. The curve drawn is to guide the eye and not a fit to the data.

the particle size vs SHG efficiency plots indicate that two compounds are phase matchable in both visible and ultraviolet region (Figure 3). The SHG effects of compounds **1**−**4** originate mainly from contributions of the BO_3 units with small contributions of BO_4 tetrahedra and π-conguated CH_3COO^- anions based on the anionic group theory.[31,32]

Ferroelectric Properties. Because of their polar structures, it is worth investigating the ferroelectric properties for compounds **1**−**4**. Hysteresis loops of compounds **1**−**4** display small remnant polarizations (Pr) of 0.020, 0.016, 0.013, and 0.022 $\mu C/cm^2$, respectively, hence the ferroelectric properties are negligible (SI Figure S7). The polarization reversibility could arise from the dielectric loss.

Theoretical Calculations. To understand more clearly the origins of the SHG effects for compounds **1**−**4**, the theoretical investigations on the compound **4** were done as a representative. The band structure graph (Figure 4a) of

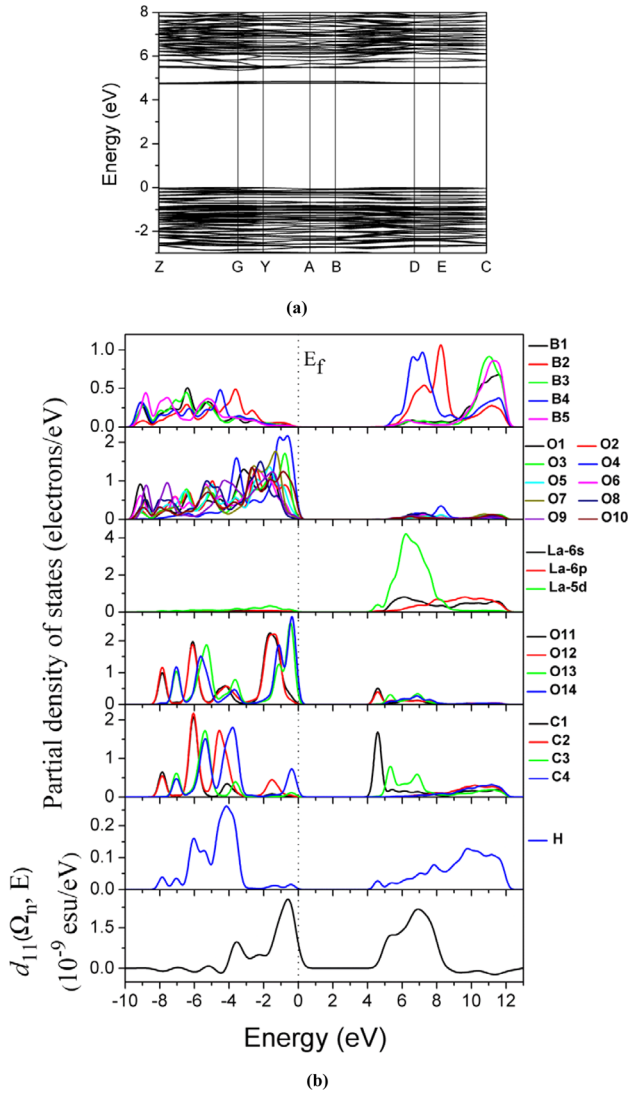

Figure 4. Calculated band structure (a) and the partial density of states (the upper six panels) and spectral decomposition of d_{11} (the bottommost panel) (b) for compound **4**.

compound **4** exhibits an indirect band gap feature (from G of VBM to near Z point of CBM) and the state energies

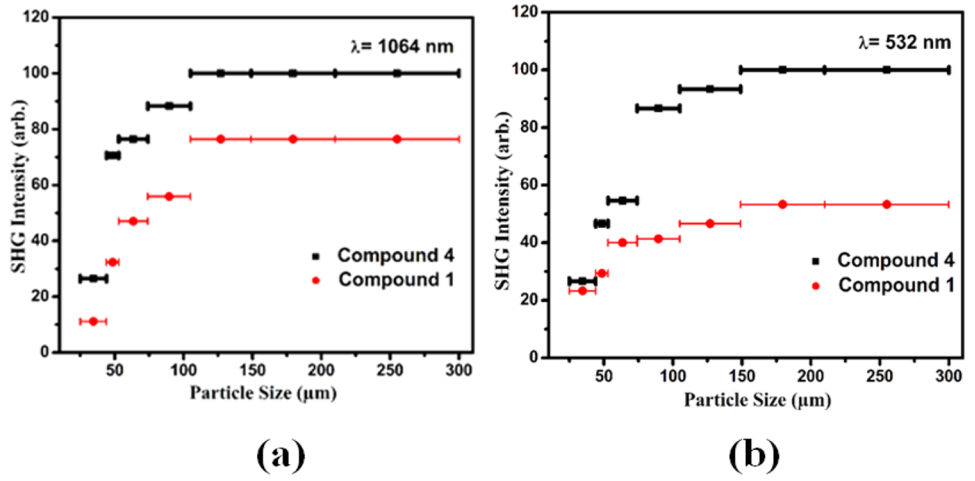

Figure 3. Phase-matching curves of compounds **1** and **4** under a 1064 nm (a) and 532 nm (b) laser radiation.

DOI: 10.1021/acs.inorgchem.5b01126
Inorg. Chem. 2015, 54, 7516−7523

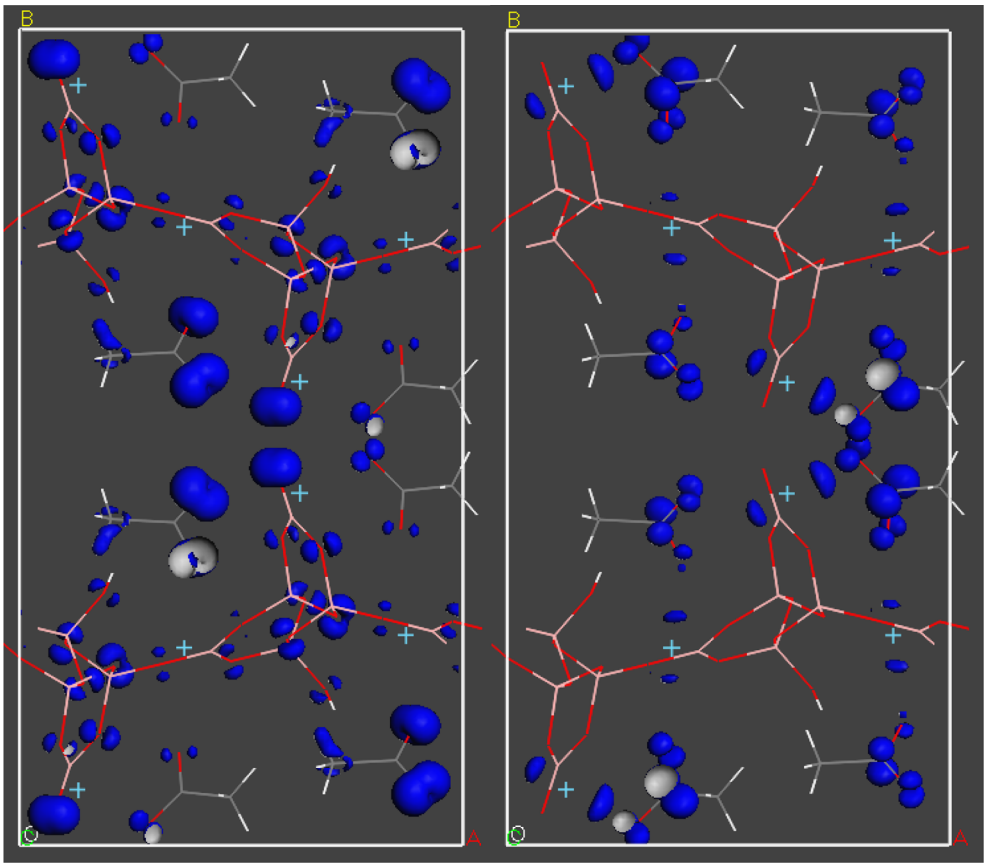

(a) (b)

Figure 5. SHG density of d_{11} in VB and CB of compound **4**.

(electronvolts) of the lowest conduction band and the highest valence band are summarized in SI Table S3. The theoretical band gap is 4.733 eV. The slightly smaller gap compared to experimental one (5.38 eV) is caused by the limitation of the exchange correlation function of GGA within DFT method.

The partial densities of states are presented in Figure 4b. From the PDOS, the bonding properties among atoms can be clearly observed. As shown in the above structure descriptions, the CH_3COO^- and the $[B_5O_{11}(OH)]^{8-}$ groups that seem to be separated from each other are further linked through La−O bonds. That is confirmed by the fact that the La-5d has an obvious overlap with all O atoms in the PDOS graph. For CH_3COO^-, it can be seen that there are strong covalent bonding interactions of C−H, C_1−C_2, C_3−C_4, C_1−O_{11}, C_1−O_{12}, C_3−O_{13}, and C_3−O_{14} bonds. All the peaks in the CH_3COO^- group marked by C_1, C_2 are red-shifted compared to those labeled by C_3, C_4. This is because the O_{12}-2p orbitals match the La_1-d_{xy} orbitals very well in direction, and there are stronger bonding interactions in La_1−O_{12} than in La−O_{13}/O_{14}. As a result, more La-5d electrons participate in O_{12}-2p nonbonding orbitals and make the corresponding states energies shift downward. For $[B_5O_{11}(OH)]^{8-}$ group, the states in the ranges of −9.6 to −4.8 eV and 9.5−12.1 eV are from the σ bonding and σ^* antibonding of B and O atoms, respectively. Some states of −4.8 to −2.2 eV and 5.9−8.9 eV correspond to the π bonding and π^* antibonding of B_2/B_4−O bonds. Most valence states close to the Fermi level are dominated by the O-2p nonbonding electronic states, especially the terminal O atoms (O_4, O_{13}, and O_{14}, etc.), whether it is in $[B_5O_{11}(OH)]^{8-}$ or CH_3COO^- group. The bottommost conduction states, corresponding to the several isolated bands in band structure, are mainly from C_1. Hence the band gap of compound **4** is determined by the CH_3COO^- groups (Figure 4b).

The second-order susceptibilities of compound **4** in the static limit are calculated, as listed in SI Table S4. The highest tensor d_{11} of compound **4** is 4.37×10^{-9} esu, slightly larger than the experimental value (2.5 × KDP for compound **4**). Because of the component complexity of the compound (except for the common borates groups, there is organic CH_3COO^- group in the structure), it is crucial to explore the SHG response origin theoretically. It is very important to show clearly which energy levels of electronic states give contributions to the SHG effect, so we performed the spectral decomposition of the highest SHG coefficient d_{11} in the static limit, as plotted in the bottommost panel of Figure 4b. Obviously, the energy regions of −1.7−0 eV in VB and 4.5−8.5 eV in CB give the most contributions, and the region of −4.2 to −1.7 eV in VB also gives some positive contributions to the SHG effect. These contributed regions correspond to some electronic states in energy. To accurately reveal which electronic states contribute to the SHG effect, we calculate the SHG density, which can provide an intuitive orbital image for the SHG contributions and had successfully interpreted the SHG effects origins for our previously reported crystals.[11,33] The SHG density graphs of d_{11} in VB and CB for compound **4** are displayed in Figure 5. The largest contribution in VB comes from the terminal O-2p nonbonding states, especially in O_4, O_{13}, and O_{14}, which have the strongest DOS peaks in VBM. The second largest

DOI: 10.1021/acs.inorgchem.5b01126
Inorg. Chem. 2015, 54, 7516−7523

contribution is from the nonbonding states of O_3, O_7, O_{10}, and O_{11}. The SHG contribution in CB is mainly at the delocalized π^* antibonding states of C−O bonds, and the unoccupied La-5d orbitals also give a few of contributions in CB. The integrals over the whole energy range (including VB and CB) can give the contribution percents to SHG effect from each group or ion. For compound **4**, the percentages of the SHG contributions from $[B_5O_{11}(OH)]^{8-}$, CH_3COO^- anions, and La^{3+} ions are calculated to be 38.11%, 41.10% and 19.74%, respectively. The results indicate that in the compound, except for the common borates groups, CH_3COO^- groups also play an important part in SHG process because of its partly planar and delocalized π bonds. In addition, La^{3+} ions make contribution to SHG responses which can not be ignored.

CONCLUSIONS

In summary, the first examples of noncentrosymmetric lanthanide borate−acetate hybrids, namely, $Ln_2(CH_3CO_2)_2[B_5O_9(OH)]\cdot H_2O$ (Ln = La **1**; Ce **2**; Pr **3**) and $Ln_2(CH_3CO_2)_2[B_5O_9(OH)]$ (Ln = La **4**; Ce **5**; Pr **6**), have been prepared successfully. Their structures feature a novel 3D lanthanide (III) borate network decorated by acetate anions. Single crystal to single crystal dehydrations from compounds **1**−**3** to compounds **4**−**6** have been observed. Compounds **1**−**4** show moderate SHG responses under laser radiation at both 1064 and 532 nm, and they are all phase-matching. The relatively large SHG coefficients of these compounds originate from the synergistic effect of π-conjugated $[BO_3]^{3-}$ units and CH_3COO^- units. It is expected that a large number of other SHG-active hybrid materials can be synthesized by the combination of borate clusters with π-conjugated organic ligands.

ASSOCIATED CONTENT

Supporting Information

X-ray crystallographic files in CIF format, selected bond distances, SHG tensors, state energies (electronvolts) of the lowest conduction band (L-CB) and the highest valence band (H-VB), simulated and experimental XRD patterns, TGA and DSC curves, IR spectra, UV spectra, optical diffuse reflectance spectra, and ferroelectric properties for compounds **1**−**4**. The Supporting Information is available free of charge on the ACS Publications website at DOI: 10.1021/acs.inorgchem.5b01126.

AUTHOR INFORMATION

Corresponding Author

* Fax: +86 591-83714946. E-mail: mjg@fjirsm.ac.cn.

Notes

The authors declare no competing financial interest.

ACKNOWLEDGMENTS

Our work was supported by National Natural Science Foundation of China (Grants 21231006, 21373222, and 21401194).

REFERENCES

(1) (a) Ok, K. M.; Chi, E. O.; Halasyamani, P. S. *Chem. Soc. Rev.* **2006**, *35*, 710−717. (b) Chen, C. T.; Liu, G. Z. *Annu. Rev. Mater. Sci.* **1986**, *16*, 203−243. (c) Ok, K. M.; Chi, E. O.; Halasyamani, P. S. *Chem. Soc. Rev.* **2006**, *35*, 710−717.

(2) (a) Hagerman, M. E.; Poeppelmeier, K. R. *Chem. Mater.* **1995**, *7*, 602−621. (b) Eaton, D. F. *Science* **1991**, *253*, 281−287.

(3) (a) Sasaki, T.; Mori, Y.; Yoshimura, M.; Yap, Y. K.; Kamimura, T. *Mater. Sci. Eng., R* **2000**, *30*, 1. (b) Zhao, S. G.; Gong, P. F.; Bai, L.; Xu, X.; Zhang, S. G.; Sun, Z. H.; Lin, Z. S.; Hong, M. C.; Chen, C. T.; Luo, J. H. *Nat. Commun.* **2014**, *5*, 4019.

(4) (a) Becker, P. *Adv. Mater.* **1998**, *10*, 979−992. (b) Hagerman, M. E.; Poeppelmeier, K. R. *Chem. Mater.* **1995**, *7*, 602−621. (c) Mori, Y.; Kuroda, I.; Nakajima, S.; Sasaki, T.; Nakai, S. *Appl. Phys. Lett.* **1995**, *67*, 1818−1820.

(5) (a) Chen, C. T.; Wu, Y. C.; Li, R. K. *Int. Rev. Phys. Chem.* **1989**, *8*, 65−91. (b) Chen, C. T.; Liu, G. Z. *Annu. Rev. Mater. Sci.* **1986**, *16*, 203−243.

(6) (a) Song, J. L.; Hu, C. L.; Xu, X.; Kong, F.; Mao, J. G. *Angew. Chem., Int. Ed.* **2015**, *54*, 3679−3682. (b) Abudoureheman, M.; Wang, L.; Zhang, X.; Yu, H.; Yang, Z.; Lei, C.; Han, J.; Pan, S. L. *Inorg. Chem.* **2015**, *54*, 4138−4142.

(7) (a) Guo, Z. G.; Cao, R.; Wang, X.; Li, H. F.; Yuan, W. B.; Wang, G. J.; Wu, H. H.; Li, J. *J. Am. Chem. Soc.* **2009**, *131*, 6894−6895. (b) Reinsch, H.; van der Veen, M. A.; Gil, B.; Marszalek, B.; Verbiest, T.; de Vos, D.; Stock, N. *Chem. Mater.* **2013**, *25*, 17−26.

(8) Evans, O. R.; Lin, W. *Acc. Chem. Res.* **2002**, *35*, 511−522.

(9) Dang, S.; Zhang, J. H.; Sun, Z. M.; Zhang, H. *Chem. Commun.* **2012**, *48*, 11139−11141.

(10) (a) Wang, C.; Zhang, T.; Lin, W. *Chem. Rev.* **2012**, *112*, 1084−1104. (b) Lin, W. B.; Lin, W. P.; Wong, G. K.; Marks, T. J. *J. Am. Chem. Soc.* **1996**, *118*, 8034−8042. (c) Yu, J.; Cui, Y.; Wu, C.; Yang, Y.; Wang, Z.; O'Keeffe, M.; Chen, B.; Qian, G. *Angew. Chem., Int. Ed.* **2012**, *51*, 10542−10545.

(11) Isakov, D.; de Matos Gomes, E.; Belsley, M. S.; Rodrigues, V. H.; Ramalho Costa, M. M. *CrystEngComm* **2012**, *14*, 3767−3771.

(12) Gómez-Aguirre, L. C.; Pato-Doldán, B.; Stroppa, A.; Yáñez-Vilar, S.; Bayarjargal, L.; Winkler, B.; Castro-García, S.; Mira, J.; Sánchez-Andújar, M.; Señarís-Rodríguez, M. A. *Inorg. Chem.* **2015**, *54*, 2109−2116.

(13) Fu, D. F.; Zhang, W.; Xiong, R. G. *Dalton Trans.* **2008**, 3946−3948.

(14) Park, Y.; Advincula, R. C. *Chem. Mater.* **2011**, *23*, 4273−4294.

(15) (a) Park, Y.; Advincula, R. C. *Chem. Mater.* **2011**, *23*, 4273−4294. (b) Yamamoto, K.; Tatsumi, T. *Chem. Mater.* **2008**, *20*, 972−980.

(16) (a) Fan, X.; Pan, S.; Guo, J.; Hou, X.; Han, J.; Zhang, F.; Li, F.; Poeppelmeier, K. R. *J. Mater. Chem. A* **2013**, *1*, 10389−10394.

(17) (b) Chen, Z. H.; Pan, S. J.; Wu, H. P.; Yang, Y.; Fan, X. Y. *Mater. Chem. Phys.* **2011**, *129*, 649−653.

(18) (a) Aka, G.; Kahn-Harari, A.; Mougel, F.; Vivien, D.; Salin, F.; Coquelin, P.; Colin, P.; Pelenc, D.; Damelet, J. L. *J. Opt. Soc. Am. B* **1997**, *14*, 223−225. (b) Aka, G.; Kahn-Harari, A.; Vivien, D.; Benitez, J. M.; Salin, F.; Godard, J. *Eur. J. Solid State Inorg. Chem.* **1996**, *33*, 727−736. (c) Polinski, M. J.; Wang, S.; Alekseev, E. V.; Depmeier, W.; Albrecht-Schmitt, T. E. *Angew. Chem., Int. Ed.* **2011**, *50*, 8891−8894.

(19) (a) Fang, S. H.; Liu, H.; Ye, N. *Cryst. Growth Des.* **2011**, *11*, 5048−5052. (b) Pei, Z. W.; Su, Q.; Zhang, J. Y. *J. Alloys Compd.* **1993**, *198*, 51−53. (c) Huppertz, H.; von der Eltz, B. *J. Am. Chem. Soc.* **2002**, *124*, 9376−9377. (d) Saubat, B.; Fouassier, C.; Hagenmuller, P.; Bourcet, J. C. *Mater. Res. Bull.* **1981**, *16*, 193−198.

(20) (a) Belokoneva, E. L.; Azizov, A. V.; Leonyuk, N. I.; Simonov, M. A. *J. Struct. Chem.* **1981**, *22*, 476−477. (b) Luo, M.; Ye, N.; Zou, G. H.; Lin, C. S.; Cheng, W. D. *Chem. Mater.* **2013**, *25*, 3147−3153. (c) Ren, M.; Lin, J. H.; Dong, Y.; Yang, L. Q.; Su, M. Z.; You, L. P. *Chem. Mater.* **1999**, *11*, 1576−1580. (d) Li, L. Y.; Jin, X. L.; Li, G. B.; Wang, Y. X.; Liao, F. H.; Yao, G. Q.; Lin, J. H. *Chem. Mater.* **2003**, *15*, 2253−2260.

(21) (a) Mills, A. D. *Inorg. Chem.* **1962**, *1*, 960−961. (b) Ballman, A. A. *Am. Mineral.* **1962**, *47*, 1380−1383. (c) Polinski, M. J.; Grant, D. J.; Wang, S.; Alekseev, E. V.; Cross, J. N.; Villa, E. M.; Depmeier, W.; Gagliardi, L.; Albrecht-Schmitt, T. E. *J. Am. Chem. Soc.* **2012**, *134*, 10682−10692. (d) Wang, S.; Alekseev, E. V.; Stritzinger, J. T.; Depmeier, W.; Albrecht-Schmitt, T. E. *Inorg. Chem.* **2010**, *49*, 6690−6696. (e) Polinski, M. J.; Wang, S.; Alekseev, E. V.; Depmeier, W.; Albrecht-Schmitt, T. E. *Angew. Chem., Int. Ed.* **2011**, *50*, 8891−8894.

DOI: 10.1021/acs.inorgchem.5b01126
Inorg. Chem. 2015, 54, 7516−7523

(22) Kurtz, S. K.; Perry, T. T. *J. Appl. Phys.* **1968**, *39*, 3798−3813.
(23) (a) *CrystalClear*, v. 1.3.5; Rigaku Corp.: Woodlands, TX, 1999. (b) Sheldrick, G. M. *SHELXTL, Crystallographic Software Package*, v. 5.1; Bruker-AXS: Madison, WI, 1998. (c) Spek, A. L. *PLATON*; Utrecht University: Utrecht, The Netherlands, 2001.
(24) (a) Segall, M. D.; Lindan, P. J. D.; Probert, M. J.; Pickard, C. J.; Hasnip, P. J.; Clark, S. J.; Payne, M. C. *J. Phys.: Condens. Matter* **2002**, *14*, 2717−2744. (b) Milman, V.; Winkler, B.; White, J. A.; Pickard, C. J.; Payne, M. C.; Akhmatskaya, E. V.; Nobes, R. H. *Int. J. Quantum Chem.* **2000**, *77*, 895−910.
(25) Perdew, J. P.; Burke, K.; Ernzerhof, M. *Phys. Rev. Lett.* **1996**, *77*, 3865−3868.
(26) Lin, J. S.; Qteish, A.; Payne, M. C.; Heine, V. *Phys. Rev. B: Condens. Matter Mater. Phys.* **1993**, *47*, 4174−4180.
(27) Lin, J.; Lee, M. H.; Liu, Z. P.; Chen, C. Y.; Pickard, C. J. *Phys. Rev. B: Condens. Matter Mater. Phys.* **1999**, *60*, 13380−13389.
(28) (a) Brese, N. E.; O'Keeffe, M. *Acta Crystallogr., Sect. B: Struct. Sci.* **1991**, *47*, 192−197. (b) Brown, I. D.; Altermatt, D. *Acta Crystallogr., Sect. B: Struct. Sci.* **1985**, *41*, 240−244.
(29) Wei, Q.; Cheng, J. W.; He, C.; Yang, G. Y. *Inorg. Chem.* **2014**, *53*, 11757−11763.
(30) Hu, T.; Qin, L.; Kong, F.; Zhou, Y.; Mao, J. G. *Inorg. Chem.* **2009**, *48*, 2193−2199.
(31) (a) Chen, C. T.; Wu, Y. C.; Li, R. C. *J. Cryst. Growth* **1990**, *99*, 790−798. (b) Yu, H. W.; Wu, H. P.; Pan, S. L.; Yang, Z.; Su, X.; Zhang, F. F. *J. Mater. Chem.* **2012**, *22*, 9665−9670. (c) Yang, Y.; Pan, S.; Han, J.; Hou, X.; Zhou, Z.; Zhao, W.; Chen, Z.; Zhang, M. *Cryst. Growth Des.* **2011**, *11*, 3912−3916. (d) Hu, C. L.; Xu, X.; Sun, C. F.; Mao, J. G. J. *J. Phys.: Condens. Matter* **2011**, *23*, 395501.
(32) (a) Shi, Y. J.; Pan, S. L.; Dong, X. Y.; Wang, Y.; Zhang, M.; Zhang, F. F.; Zhou, Z. X. *Inorg. Chem.* **2012**, *51*, 10870−10875. (b) Izumi, H. K.; Kirsch, J. E.; Stern, C. L.; Poeppelmeier, K. R. *Inorg. Chem.* **2005**, *44*, 884−895. (c) Yang, H.; Hu, C. L.; Song, J. L.; Mao, J. G. *RSC Adv.* **2014**, *4*, 45258−45265.
(33) Xu, X.; Hu, C. L.; Li, B. X.; Yang, B. P.; Mao, J. G. *Chem. Mater.* **2014**, *26*, 3219−3230.

DOI: 10.1021/acs.inorgchem.5b01126
Inorg. Chem. 2015, 54, 7516−7523